Preprint, 11th IFAC Symposium on Dynamics and Control of Process Systems,
including Biosystems
June 6-8, 2016. NTNU, Trondheim, Norway

Optimal Health-aware Charging Protocol for Lithium-ion Batteries: A Fast Model Predictive Control Approach

M. Torchio * **L. Magni** * **R.D. Braatz** ** **D.M. Raimondo** ***

* *Dipartimento di Ingegneria Civile e Architettura, University of Pavia, 27100 Pavia, Italy (e-mail marcello.torchio01@ateneopv.it, lalo.magni@unipv.it)*
** *Massachusetts Institute of Technology, Cambridge, MA, United States of America 02142 (e-mail: braatz@mit.edu)*
*** *Dipartimento di Ingegneria Industriale e dell'Informazione University of Pavia, 27100 Pavia, Italy (e-mail: davide.raimondo@unipv.it)*

Abstract: Lithium-ion batteries are widely used in industry to supply different portable applications. Their management is handled by Battery Management Systems (BMSs), which are intended to ensure good performance (such as minimum charging time) while simultaneously minimizing safety risks. The use of accurate mathematical models can help in achieving such goals. The first-principles pseudo-two dimensional (P2D) model is one of the mostly used models for simulation but rarely used in design of BMSs. This model, together with a description of the capacity fade mechanisms occurring during battery operations, is used to design health-aware BMS strategies. A Model Predictive Control (MPC) scheme based on a linearized version of the P2D model is proposed in order to track a reference value of the State of Charge (SOC), while taking into account the aging dynamics of the system as well as temperature and voltage constraints. Simulations show the effectiveness of the approach: the tuning of the control parameters allows controlled operation with different tradeoffs between charging time and battery lifetime enhancement.

Keywords: Advanced Battery Management Systems, health-aware control of Li-ion batteries, model predictive control

1. INTRODUCTION

In the past decades, the ever increasing usage of consumer electronics, hybrid and electric vehicles, and energy storage devices has resulted in a significant demand for reliable and high-performance electrochemical accumulators. Different chemistries have been developed, including nickel-cadmium batteries (NiCd), nickel-metal hydride batteries (NiMh), lead-acid batteries, and Li-ion accumulators. Among the different technologies, Li-ion batteries exhibit the best tradeoff in terms of power capacity, energy density, high open-circuit voltage, and wide temperature operations (for example, see Besenhard (2008) and Van den Bossche et al. (2006)). The use of detailed mathematical models allows the design of better batteries and improved Battery Management Systems (BMSs). The two main classes of models are used in literature for describing Li-ion batteries are the Equivalent Circuit Models (ECMs), and the Electrochemical Models (EMs) (for further details see Ramadesigan et al. (2012) and references therein). ECMs require less computational effort, whereas EMs are able to represent the electrochemical phenomena more precisely.

This paper relies on the first-principles pseudo two-dimensional (P2D) electrochemical model. Based on concentrated solution theory, the P2D model was developed by Doyle et al. (1993) and allows the simulation of different chemistries and material compositions. Long-term degradation effects occurring during battery operations are also important when designing BMSs. The modeling of these effects has been addressed by many authors in the recent years (for example, see Sankarasubramanian and Krishnamurthy (2012), Zhang and White (2008)). Among them, a first-principles model able to accurately describe the capacity fade mechanisms has been proposed in Ramadass et al. (2003). This model is able to reproduce: (i) the formation of the Solid-Electrolyte Interface (SEI) layer, which results in an additional and variable resistance between the electrolyte and active material (anode), and (ii) the capacity fade effects which lead to a continuous loss of capacity during the battery cycling.

The objective of this paper is to design an Advanced Battery Management System (ABMS) for Li-ion batteries using the P2D model in combination with a description of the capacity fade mechanisms. The inclusion of the latter mechanisms allows the design of health-aware charging strategies. The ABMS proposed in this work is based on the Quadratic Dynamic Matrix Control (QDMC) algorithm (Garcia and Morshedi (1986)). Since QDMC requires the solution of a constrained optimization at each time step, its online application can be prohibitive when

high-order and nonlinear models are considered. For this reason, the controller in this work is computed according to a linearized input-output version of the P2D model. The adoption of such a model significantly reduces the computational burden without compromising the control performance. Differently from our previous work (Torchio et al. (2015)), the inclusion of the aging dynamics allows the design of a health-aware charging protocol by adding soft constraints on the battery capacity fade on top of the already existing constraints on voltage and temperature. In simulations, the proposed approach shows that different tradeoffs between battery aging and minimum time charging can be obtained by properly tuning the control parameters.

2. LI-ION BATTERY MODEL

This section recalls the P2D model. To consider battery aging, the model is augmented with dynamics describing the capacity fade effects and the formation of the Solid-Electrolyte Interface layer at the electrolyte-anode interface. A Li-ion cell is composed of five main sections: the positive current collector (a), the cathode (p), the separator (s), the anode (n), and the negative current collector (v). The index $z \in \{a, p, s, n, v\}$ is used to indicate the different sections. The thickness of each battery section is defined by L_z and $L := \sum_z L_z$ represents the overall battery thickness. The electrodes and the porous separator of the Li-ion cell are placed in contact with an electrolyte solution, facilitating the flow of ions during charging and discharging processes. During a charging process, the ions deintercalate from the positive electrode and, passing through the porous media of the separator, intercalate into the negative electrode. The inverse process occurs when discharging the cell. The diffusion of ions within the electrodes is modeled by

$$\frac{\partial}{\partial t} c_s^{\text{avg}}(x,t) = -\frac{3}{R_s} j(x,t) \tag{1}$$

$$c_s^*(x,t) - c_s^{\text{avg}}(x,t) = -\frac{R_s}{5 D_{\text{eff}}^s} j(x,t), \tag{2}$$

where $t \in \mathbb{R}^+$ represents the time, $x \in \mathbb{R}$ is the one-dimensional spatial variable, $c_s^*(x,t)$ and $c_s^{\text{avg}}(x,t)$ are the surface and average concentration of solid particles respectively, the function $j(x,t)$ represents the ionic flux, and R_s and D_{eff}^s account for the particle radius and effective diffusion coefficients of the solid phases. The bulk State of Charge (SOC) of the anode is defined as

$$\text{SOC}(t) := \frac{1}{L_n \, c_s^{\text{max,n}}} \int_0^{L_n} c_s^{\text{avg}}(x,t)\, dx,$$

where $c_s^{\text{max,n}}$ represents the maximum concentration of Li-ions in the negative electrode. The flow of ions inside the electrolyte solution is modeled by a diffusion equation,

$$\epsilon \frac{\partial}{\partial t} c_e(x,t) = \frac{\partial}{\partial x}\left[D_{\text{eff}} \frac{\partial c_e(x,t)}{\partial x} \right] + a(1-t_+) j(x,t), \tag{3}$$

where $c_e(x,t)$ represents the electrolyte concentration of ions, t_+ defines the transference number, a is the particle surface area to volume ratio, D_{eff} accounts for the effective diffusion coefficients in the electrolyte, and ϵ represents the material porosity. According to Ohm's law, the conservation of charge in the electrodes can be defined as

$$\frac{\partial}{\partial x}\left[\sigma_{\text{eff}} \frac{\partial}{\partial x} \Phi_s(x,t) \right] = aFj(x,t), \tag{4}$$

where $\Phi_s(x,t)$ is the solid potential, σ_{eff} is the electrodes effective conductivity, and F is the Faraday's constant. The potential of the Li-ion cell is obtained as

$$V_{\text{out}}(t) := \Phi_s(0,t) - \Phi_s(L,t).$$

Similarly, a modified Ohm's law is used to represent the charge conservation within the electrolyte:

$$\begin{aligned} aFj(x,t) = &-\frac{\partial}{\partial x}\left[\kappa_{\text{eff}} \frac{\partial}{\partial x} \Phi_e(x,t) \right] \\ &+ \frac{\partial}{\partial x}\left[\frac{2\kappa_{\text{eff}} \text{R} T(x,t)}{F} (1-t_+) \frac{\partial}{\partial x} \ln c_e(x,t) \right], \end{aligned} \tag{5}$$

where $\Phi_e(x,t)$ is the electrolyte potential, $T(x,t)$ represents the temperature, R defines the universal gas constant, and κ_{eff} is the effective conductivity of the liquid phase. The temperature dynamics are modeled by an energy balance,

$$\begin{aligned} \rho C_p \frac{\partial}{\partial t} T(x,t) = &\frac{\partial}{\partial x}\left[\lambda \frac{\partial}{\partial x} T(x,t) \right] + Q_{\text{ohm}}(x,t) \\ &+ Q_{\text{rxn}}(x,t) + Q_{\text{rev}}(x,t), \end{aligned} \tag{6}$$

where ρ is the material density, C_p is the specific heat, λ is the heat diffusion coefficient, and the terms $Q_{\text{ohm}}(x,t)$, $Q_{\text{rev}}(x,t)$, and $Q_{\text{rxn}}(x,t)$ account for ohmic, reversible, and reaction heat sources as shown in Kumaresan et al. (2008).

The above equations are coupled by means of the ionic flux, which is defined as

$$j(x,t) = j_{\text{int}}(x,t) + j_{\text{side}}(x,t),$$

where $j_{\text{int}}(x,t)$ is used to model the electrode kinetics of intercalation/deintercalation, and $j_{\text{side}}(x,t)$ accounts for side reactions during the charging of the battery. Given that the side reactions are considered to occur only at the electrolyte-anode interface, the contribution of $j_{\text{side}}(x,t)$ at the cathode side is null and no SEI resistance between cathode and electrolyte is considered. As in Ramadass et al. (2004), the side reaction flux is modeled using a Tafel relation:

$$j_{\text{side}}(x,t) = -\frac{i_{0,\text{side}}(t)}{F} \exp\left(\frac{0.5F}{\text{R}T(x,t)} \eta_{\text{side}} \right), \tag{7}$$

where $i_{0,\text{side}}(t)$ is the side reaction exchange current and η_{side} is the side reaction overpotential defined as

$$\eta_{\text{side}} := \Phi_s(x,t) - \Phi_e(x,t) - U_{\text{SEI}} - Fj(x,t) R_f(t),$$

where the term U_{SEI} represents the side reaction Open Circuit Voltage (OCV) and $Fj(x,t)R_f(t)$ accounts for an extra voltage drop due to the presence of the SEI resistance $R_f(t)$. The growth of the SEI layer is modeled as

$$\frac{\partial}{\partial t} \delta(x,t) = -\frac{M_w}{\rho} j_{\text{side}}(x,t), \tag{8}$$

where M_w is the molar weight of the electrode and $\delta(x,t)$ represents the film thickness. The overall film resistance is given by

$$R_f(t) = R_{\text{SEI}} + \frac{\bar{\delta}(t)}{\nu},$$

where R_{SEI} is the initial SEI layer resistance, $\bar{\delta}(t)$ is the spatial mean of $\delta(x,t)$ and ν is the admittance of the film.

The side reaction exchange current $i_{0,\text{side}}(t)$ depends on the battery applied current density $I_{\text{app}}(t)$ (Rashid and Gupta (2014)). No experimental data are available for the identification of such relation, and the empirical equation

$$i_{0,\text{side}}(t) = i_{0,\text{base}} \left(\frac{I_{\text{app}}(t)}{I_{1C}} \right)^{w} \tag{9}$$

is adopted. At the anode side, due to the presence of the SEI layer, the diffusion process of Li-ions within the electrode (1),(2) is driven from $j(x,t) = j_{\text{int}}(x,t)$. The intercalation flux is governed by the Butler-Volmer equation

$$j_{\text{int}}(x,t) = 2\frac{i_{0,\text{int}}}{F} \sinh\left[\frac{0.5F}{\text{R}T(x,t)} \eta_{\text{int}} \right], \tag{10}$$

where the exchange current density is given by

$$i_{0,\text{int}} = Fk_{\text{eff}} \sqrt{c_e(x,t)(c_s^{\max} - c_s^*(x,t))c_s^*(x,t)}.$$

The overpotential at the anode side is defined as

$$\eta_{\text{int}} := \Phi_s(x,t) - \Phi_e(x,t) - U_n - Fj(x,t)R_f(t),$$

while at the cathode side as

$$\eta_{\text{int}} := \Phi_s(x,t) - \Phi_e(x,t) - U_p$$

where the terms U_p and U_n represent the cathode and anode OCV respectively, and k_{eff} represents the effective kinetic reaction rate. The intercalation flux $j_{\text{int}}(x,t)$ is zero inside the separator.

The overall set of nonlinear and tightly coupled Partial Differential Algebraic Equations (PDAEs) is used to represent all the electrochemical phenomena occurring in the Li-ion cell. A more detailed description of the model with the complete set of equations, boundary conditions (BCs) and parameters used in this work can be found in Northrop et al. (2011). The resulting set of PDAEs together with the BCs is reformulated as a set of Differential Algebraic Equations (DAEs). The spatial domain is discretized according to the Finite Volume Method (FVM), whereas the time domain is left continuous, according to the Method of Lines (MOL) method as discussed in Schiesser (1991).

2.1 Capacity fade effects

In this work, degradation effects are considered to occur only during charging processes of the cell, as discussed in Ramadass et al. (2004). The dynamics describing the capacity fade effects can be represented by the ODE

$$\frac{\partial Q_s}{\partial t} = a_n F \int_0^{L_n} j_{\text{side}}(x,t)dx,$$

where $Q_s(t)$ accounts for the capacity fading as a function of the side reaction flux. At the end of each charge cycle N_c, an estimate of the overall lost capacity is computed as

$$Q_s^{N_c} = Q_s(t_f)$$

where t_f represents the duration of the charging cycle. Before starting the next discharging cycle, the initial concentration of the anode is updated by

$$c_s^{\text{avg,init}}\big|_{N_c+1} = c_s^{\text{avg,init}}\big|_{N_c} - \frac{Q_s^{N_c}}{F\epsilon_n L_n}.$$

According to this scheme, the long-term degradation effects considered in this work produce a reduction of the cell capacity after each charging cycle.

3. MODEL IDENTIFICATION FOR ONLINE CONTROL

Predictive control algorithms require the solution, at each time step, of a constrained optimization. Solving these problems, online and quickly, becomes intractable when high-order nonlinear systems are considered. To overcome this limitation, input-output models can be used to dramatically reduce the computational burden while still providing good performance. This work employs a particular family of input-output models known as Finite Step Response (FSR) models.

3.1 Finite Step Response (FSR) models

Linear models can be represented by means of different formulations such as state-space, finite impulse response, and autoregressive exogenous models. Among the models, the family of linear input-output Finite Step Response (FSR) models is widely used in industrial applications. According to this model, the output of a system at time step k can be written in terms of FSR coefficients and input variations as

$$y_k^l = y_{ss}^l + \sum_{h=1}^{N_u-1} \left(\sum_{i=1}^{N-1} G_{h,l}^i \Delta u_{k-i}^h + G_{h,l}^N (u_{k-N}^h - u_{ss}^h) \right) \tag{11}$$

where y_{ss}^l and u_{ss}^h represent, respectively, the lth component of the steady output and hth component of the steady input, Δu_k indicates the difference $u_k - u_{k-1}$, and $G_{h,l}^k$ represents the FSR coefficient at time step k relating the hth input to the lth output. For asymptotically stable systems $G_{h,l}^N \approx G_{h,l}^{N+1} \approx \cdots \approx G_{h,l}^{\infty}$, where N represents the settling time. Similarly, for integrating plants, the output response becomes a pure ramp after N steps.

3.2 FSR model identification

When dealing with generic nonlinear plants, identification techniques can be applied to find a suitable set of FSR coefficients describing the plant dynamics. This work computes the set of FSR coefficients using a least-squares (LS) identification. Consider a nonlinear MIMO plant having a set of manipulated variables $\mathcal{M} := \{1, 2, \cdots, N_u\}$ and measured variables $\mathcal{O} := \{1, 2, \cdots, N_y\}$, which is driven to a steady output $y_{ss} \in \mathbb{R}^{N_y}$ by applying $u_{ss} \in \mathbb{R}^{N_u}$. For each input-output relationship $(m, o) \in \mathcal{M} \times \mathcal{O}$, a set of FSR coefficients has to be estimated. Assume the application of $u^{\bar{m}}$ to the $\bar{m}$th input channel, such that $|u^{\bar{m}} - u_{ss}^{\bar{m}}| = j^{\bar{m}}$, while leaving all the other channels $(m \neq \bar{m})$ at steady values. As a result, the data coming from the $\bar{o}$th output channel is collected and normalized with respect to $j^{\bar{m}}$. The normalized data are then collected in the array $\Upsilon_{\bar{m},\bar{o}}^{j^{\bar{m}}} \in \mathbb{R}^N$. The experiment is then repeated s times, by considering different input variations $[j_1^{\bar{m}}, j_2^{\bar{m}}, \cdots, j_s^{\bar{m}}]$, such that all the resulting experiments are collected in the array $\boldsymbol{\Upsilon}_{\bar{\boldsymbol{m}}}^{\bar{\boldsymbol{o}}} := \left[(\Upsilon_{\bar{m},\bar{o}}^{j_1^{\bar{m}}})^{\text{T}}, (\Upsilon_{\bar{m},\bar{o}}^{j_2^{\bar{m}}})^{\text{T}}, \cdots, (\Upsilon_{\bar{m},\bar{o}}^{j_s^{\bar{m}}})^{\text{T}} \right]^{\text{T}} \in \mathbb{R}^{Ns}$. The set of FSR coefficients $\boldsymbol{G}_{\bar{\boldsymbol{m}},\bar{\boldsymbol{o}}} = \left[G_{\bar{m},\bar{o}}^1 \; G_{\bar{m},\bar{o}}^2 \; G_{\bar{m},\bar{o}}^3 \; \cdots \; G_{\bar{m},\bar{o}}^N \right]^{\text{T}} \in \mathbb{R}^N$, relating the $\bar{m}$th input to the $\bar{o}$th output, is determined by minimizing

$$J(\boldsymbol{G}_{\bar{\boldsymbol{m}},\bar{\boldsymbol{o}}}) = ||\Omega \boldsymbol{G}_{\bar{\boldsymbol{m}},\bar{\boldsymbol{o}}} - \boldsymbol{\Upsilon}_{\bar{\boldsymbol{m}}}^{\bar{\boldsymbol{o}}}||_2^2$$

where $\Omega := [I_N \; I_N \; \cdots \; I_N]^{\text{T}} \in \mathbb{R}^{Ns \times N}$. The same procedure is repeated for all input and output channels.

4. HEALTH-AWARE PREDICTIVE CONTROL ALGORITHM

This paper employs a predictive control approach to design an optimal health-aware ABMS. In particular, a QDMC algorithm is adopted (see Garca et al. (1989) for a complete survey). Like all predictive control algorithms, QDMC relies on a dynamic model of the regulated plant in order to perform future predictions of the output, and optimizes performance while accounting for physical constraints on both inputs and outputs. Due to its capabilities to support and improve the manufacturing process, this algorithm has been implemented in a wide number of industrial applications (e.g., see Mesbah et al. (2015) and Peterson et al. (1992) and citations therein). For completeness, below is a summary of the QDMC algorithm for SISO systems and its extension to the MIMO case.

4.1 Output Predictions

The QDMC algorithm exploits a FSR model of the controlled plant to perform future predictions of the output. Starting from time instant k, by considering an input variation $\Delta u_{k|k}$, the one step-ahead prediction of a SISO system can be written as

$$\hat{y}_{k+1|k} = G^1_{1,1}\Delta u_{k|k} + f_{k+1|k}, \tag{12}$$

where the nomenclature $x_{q|k}$ represents the value of x at time q starting from instant k, and $f_{k+1|k}$ is the free response term. In general, $f_{k+q|k}$ represents the plant output y_{k+q} assuming that $\Delta u_{k+q} = 0,\ \forall q \geq 0$, i.e.:

$$f_{k+q|k} := y_{k+q} \text{ in case of } \Delta u_{k+q} = 0,\ \forall q \geq 0.$$

Due to the presence of uncertainties, differences between the predicted output and the measured output have to be considered. A reasonable estimation of the unmeasured disturbances is given by

$$d_{k|k} = y^{\text{meas}}_k - f_{k|k},$$

where y^{meas}_k represents the measured output at time instant k. This estimate can be incorporated into (12) to improve the prediction accuracy.

Generalize this formulation by introducing the prediction and control horizons, indicated by $H_p \geq 0$ and H_u, respectively, with $H_u \leq H_p$. In this way, the input variations are constrained to be zero after H_u time steps (i.e., $\Delta u_{k+g|k} = 0,\ \hat{y}_{k+g|k} = f_{k+g|k},\ \forall g \in (H_u + 1, \cdots, H_p)$). The disturbance-corrected predictions over the future H_p steps are given by

$$\hat{\boldsymbol{y}}_{\boldsymbol{k}} = \underbrace{\Xi \boldsymbol{f}_{\boldsymbol{k}}}_{\text{past inputs}} + \underbrace{\underline{\boldsymbol{G}}_{\mathbf{1,1}}\boldsymbol{\Delta u}_{\boldsymbol{k}}}_{\text{future actions}} + \underbrace{\boldsymbol{d}_{\boldsymbol{k}}}_{\text{correction terms}}, \tag{13}$$

where

$$\begin{aligned}
\hat{\boldsymbol{y}}_{\boldsymbol{k}} &:= \left[\hat{y}_{k+1|k}\ \hat{y}_{k+2|k}\ \cdots\ \hat{y}_{k+H_p|k}\right]^{\mathrm{T}} \in \mathbb{R}^{H_p},\\
\boldsymbol{f}_{\boldsymbol{k}} &:= \left[f_{k|k}\ f_{k+1|k}\ \cdots\ f_{k+N-1|k}\ \right]^{\mathrm{T}} \in \mathbb{R}^{N},\\
\boldsymbol{\Delta u}_{\boldsymbol{k}} &:= \left[\ \Delta u_{k|k}\ \Delta u_{k+1|k}\ \cdots\ \Delta u_{k+H_u-1|k}\ \right]^{\mathrm{T}} \in \mathbb{R}^{H_u},\\
\boldsymbol{d}_{\boldsymbol{k}} &:= \left[d_{k+1|k}\ d_{k+2|k}\ \cdots\ d_{k+H_p|k}\right]^{\mathrm{T}} \in \mathbb{R}^{H_p}.
\end{aligned}$$

The matrix $\Xi \in \mathbb{R}^{H_p \times N}$ is used as a shifting mask for the array $\boldsymbol{f}_{\boldsymbol{k}}$, while the lower triangular matrix $\underline{\boldsymbol{G}}_{\mathbf{1,1}}$ contains the FSR coefficients as

$$\underline{\boldsymbol{G}}_{\mathbf{1,1}} = \begin{bmatrix}
G^1_{1,1} & 0 & 0 & \cdots & 0\\
G^2_{1,1} & G^1_{1,1} & 0 & \cdots & 0\\
\vdots & \vdots & \vdots & \ddots & \vdots\\
G^{H_p}_{1,1} & G^{H_p-1}_{1,1} & G^{H_p-2}_{1,1} & \cdots & G^{H_p-H_u+1}_{1,1}
\end{bmatrix} \in \mathbb{R}^{H_p \times H_u}.$$

Given that disturbance estimates are obtained at time step k, it is assumed that $d_{k|k} = d_{k+1|k} = \cdots = d_{k+H_p|k}$. Finally, at each time instant k, input variations are used to update the free response array as

$$\boldsymbol{f}_{\boldsymbol{k+1}} := \Upsilon \boldsymbol{f}_{\boldsymbol{k}} + \boldsymbol{G}_{\mathbf{1,1}}\Delta u_{k|k},$$

where $\Upsilon \in \mathbb{R}^{N \times N}$ is a suitable shifting matrix for $\boldsymbol{f}_{\boldsymbol{k}}$. The free response array starts from an initial value which is represented by $\boldsymbol{f}_{\mathbf{0}} := f^{\text{init}}_0 \in \mathbb{R}^N$.

4.2 Optimal Control Law

The QDMC algorithm provides a control law which is obtained by finding an optimal input sequence $\boldsymbol{\Delta u_k}^*$ that minimizes (or maximizes) a given cost function $J(\boldsymbol{\Delta u_k})$ while enforcing input and output constraints. The high-level optimization can be stated as

$$\begin{aligned}
&\min_{\boldsymbol{\Delta u_k}} (\hat{\boldsymbol{y}}_{\boldsymbol{k}} - \boldsymbol{y_{ref}})^{\mathrm{T}} Q (\hat{\boldsymbol{y}}_{\boldsymbol{k}} - \boldsymbol{y_{ref}}) + \boldsymbol{\Delta u_k}^{\mathrm{T}} R \boldsymbol{\Delta u_k},\\
&\text{subject to } \boldsymbol{\Delta u_{min}} \leq \boldsymbol{\Delta u_k} \leq \boldsymbol{\Delta u_{max}},\\
&\qquad \boldsymbol{u_{min}} \leq \boldsymbol{u_k} \leq \boldsymbol{u_{max}},\\
&\qquad \boldsymbol{\Delta y_{min}} \leq \boldsymbol{\Delta \hat{y}_k} \leq \boldsymbol{\Delta y_{max}},\\
&\qquad \boldsymbol{y_{min}} \leq \hat{\boldsymbol{y}}_{\boldsymbol{k}} \leq \boldsymbol{y_{max}},
\end{aligned}$$

where the positive-semidefinite matrix $Q \in \mathbb{R}^{H_p \times H_p}$ is used to weigh the differences between the predicted outputs $\hat{\boldsymbol{y}}_{\boldsymbol{k}}$ and reference trajectories $\boldsymbol{y_{ref}}$, while the positive-definite matrix $R \in \mathbb{R}^{H_u \times H_u}$ is used as weighting factor for the input variations. When dealing with output constraints, it is common to have feasibility problems due to the presence of plant-model mismatches. For this reason, the output constraints are softened to ensure recursive feasibility at each time step. Exploiting (13), the optimization is alternatively stated as a Quadratic Program (QP):

$$\begin{aligned}
&\min_{\boldsymbol{\zeta}} \frac{1}{2}\boldsymbol{\zeta}^{\mathrm{T}} \tilde{\Theta}\, \boldsymbol{\zeta} + \tilde{\Gamma}\, \boldsymbol{\zeta},\\
&\text{subject to}\\
&A\, \boldsymbol{\zeta} \leq b
\end{aligned} \tag{14}$$

where the optimization variable is

$$\boldsymbol{\zeta} := \begin{bmatrix} \boldsymbol{\Delta u_k} \\ \boldsymbol{\chi} \end{bmatrix},$$

and $\boldsymbol{\chi}$ is used to soften the output constraints. The matrix A and array b are used to enforce input and output constraints. For a thorough description of the QP implementation process and constraints softening, refer to Maciejowski (2002).

4.3 Receding Horizon approach

At each time instant k, the solution of the optimization (14) leads to an optimal input sequence $\boldsymbol{\Delta u}^*_{\boldsymbol{k}}$. To provide the control action to the plant, according to the so-called Receding Horizon (RH) approach, only the first input variation is applied:

$$u_k = u_{k-1} + \Delta u^*_{k|k},$$

where $\Delta u^*_{k|k}$ is the first element of $\boldsymbol{\Delta u^*_k}$, while u_{k-1} represents the value of the input applied to the plant at time instant $k-1$.

5. SIMULATIONS

The effectiveness of the proposed health-aware control algorithm is demonstrated in this section. The system under control is a single-input multiple-output (SIMO) plant having $I_{\text{app}}(t)$ as the only control variable, while SOC(t), $T(t)$, $V_{\text{out}}(t)$ and $Q_s(t)$ as measured variables. Only the SOC(t) represents the controlled variable. The controller presented in Section 4 has been implemented to track a reference value of the SOC while fulfilling input and output constraints. As discussed in Section 4.2, output constraints are softened by means of the variable $\boldsymbol{\chi}$. In order to weight the constraint violations, extra factors are adopted, with the term γ referring to the weighting factors used to account for output violations. The FSR coefficients in Fig. 1, used for online optimizations, were estimated according to the approach outlined in Section 3.2.

All the proposed scenarios share the output constraints

$$2.5\,\text{V} \leq V_{\text{out}}(t) \leq 4.2\,\text{V},$$
$$0.8\% \leq \text{SOC}(t) \leq 95\%,$$
$$270\,\text{K} \leq T(t) \leq 320\,\text{K},$$
$$-10^{-9}\frac{\text{C}}{\text{m}^2\text{s}} \leq \Delta Q_s(t) \leq 10^{-9}\frac{\text{C}}{\text{m}^2\text{s}},$$

and the input constraints

$$0 \leq I_{\text{app}}(t) \leq I_{1_C},$$
$$-1.5\frac{\text{A}}{\text{m}^2\text{s}} \leq \Delta I_{\text{app}}(t) \leq 1.5\frac{\text{A}}{\text{m}^2\text{s}},$$

where $I_{1_C} = 29.5$ A/m^2 for this particular chemistry. To assess the effectiveness of the proposed control algorithm, the simulations have been run considering different values of $\gamma_{\Delta Q_s}$.The parameters used for the side reaction dynamics are the base-side reaction current $i_{0,\text{base}} = 8 \times 10^{-11}$ A/m^2, the film conductivity $\nu = 3.79 \times 10^{-7}$ S/m, and $w = 2$. The molar weight is obtained from the cell parameters as $M_w = 73 \times 10^{-3}$ kg/mol and the side reaction OCV is set to $U_{\text{side}} = 0.4$ V. All the other battery parameters used in this work can be found in Northrop et al. (2011). All the scenarios run with the environmental temperature of $T_{\text{ref}} = 298.15$ K. The plant simulation is performed using MATLAB with the IDA solver from the SUNDIALS suite developed by Hindmarsh et al. (2005). Due to computational costs, the sampling time of the controller has been chosen equal to 10 s, which is suitable according to the system bandwidth estimate. Prediction and control horizon have been set to $H_p = H_u = 200$ steps. In all the scenarios the QDMC controller has been set with $Q = 10$ and $R = 1$. The resulting QP problem is solved using the MATLAB quadprog solver. The simulations are performed on a Windows 10 machine with 8 Gbytes of RAM and a i5 vPro processor @2.5 GHz.

5.1 Results and Discussion

To assess the effectiveness of the proposed control algorithm, in Fig. 2 different charging protocols are computed by means of different weights of $\gamma_{\Delta Q_s}$. As it is possible

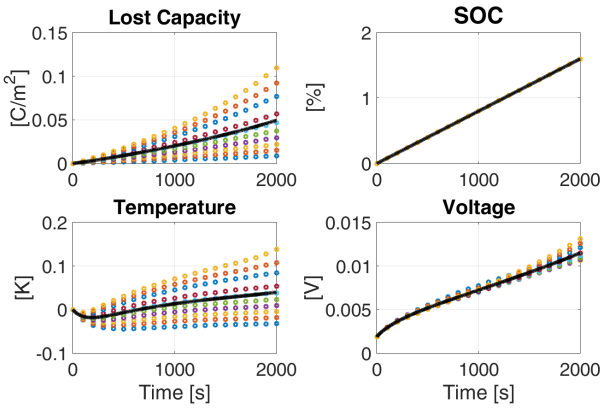

Fig. 1. FSR models: identified coefficients (black lines) and data (circles) obtained by application of the set of input variations $j^{I_{\text{app}}} \in \{5, 8, 11, 14, 17, 20, 23, 28, 31, 34, 37\}$ A/m^2, starting from a rest condition, to the battery.

to see with $\gamma_{\Delta Q_s} = 0$ (dashed purple line), the algorithm provides a charging current density which is for most of the time set to the maximum value of I_{1_C} and starts to drop when approaching the final charging stage at around 1300 s. The corresponding behavior of the output voltage shows a fast increase of $V_{\text{out}}(t)$ followed by a rest transient which settles to 3.87 V. Finally, the temperature shows a steeper increase which reaches 300 K at 1200 s and the capacity fade effect which results in a total decrease of the anode concentration of 0.35 mol/m^3. By weighting the aging dynamics in the optimization, QDMC provides more conservative control actions. The applied current profiles have different shapes according to the different weights: $\gamma_{\Delta Q_s} = 1$ (yellow line), $\gamma_{\Delta Q_s} = 5$ (dotted orange line), and $\gamma_{\Delta Q_s} = 10$ (dot-dashed blue line). By increasing $\gamma_{\Delta Q_s}$, the control action provided by QDMC is less aggressive and lasts longer. The voltage profiles show a more gentle rise during the charging process and all of them settle at 3.87 V, while temperature never goes above 298.7 K. In all the different cases, the reference value of the SOC is reached at different time instant; according to the most conservative control action, the reference is reached in 6000 s. Finally, after one charging cycle, the overall lost capacity of the most conservative profile results to be less than 1/3 of most aggressive control action. The reduction in anode capacity over multiple charging cycles are compared in Fig. 3, whereas Table 1 summarizes the lost anode capacity as a function of the cycle number. To compare the different scenarios, a common charging/discharging protocol has been defined. After 10 charging cycles, the total lost capacity is significantly reduced when aging dynamics are weighted in the optimization, which magnifies the results obtained over a single charging cycle.

Cycle #	$\gamma_{\Delta Q_s} = 0$	$\gamma_{\Delta Q_s} = 1$	$\gamma_{\Delta Q_s} = 5$	$\gamma_{\Delta Q_s} = 10$
1	0.3327	0.202	0.1362	0.1098
5	1.661	1.011	0.6829	0.5498
10	3.322	2.021	1.362	1.099

Table 1. Lost anode capacity over multiple cycles.

6. SUMMARY

An advanced battery management system (ABMS) is proposed that accounts for long-term degradation effects. A

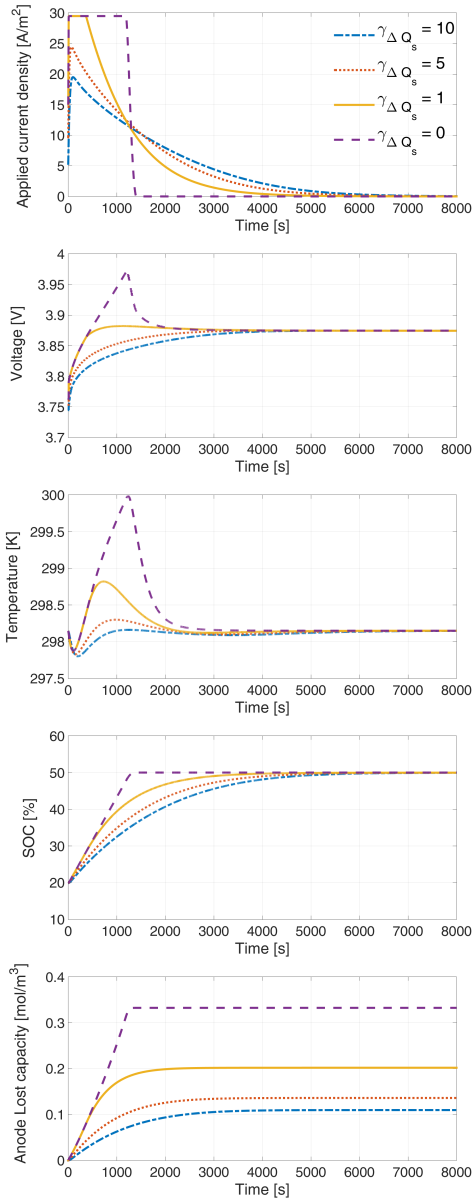

Fig. 2. Lost anode capacity for different violation weights.

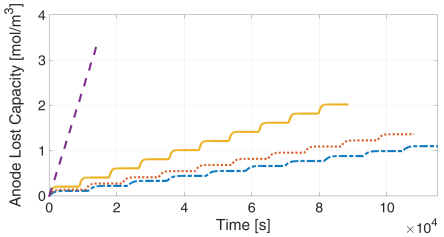

Fig. 3. Lost anode capacity over multiple cycles with different violation weights.

QDMC predictive approach is adopted to perform an optimal charge of a Li-ion cell while taking into account both input and outputs constraints. A linear representation of the Li-ion battery is employed to reduce the computational burden while still guaranteeing good control performance. Despite longer charging times, the results show significant life-cycle improvement by defining less aggressive charging protocols. The proof of principle provided by this work highlights the capabilities of predictive algorithms for use in a health-aware ABMS application.

REFERENCES

Besenhard, J.O. (2008). *Handbook of Battery Materials*. John Wiley & Sons.

Doyle, M., Fuller, T.F., and Newman, J. (1993). Modeling of galvanostatic charge and discharge of the lithium/polymer/insertion cell. *Journal of the Electrochemical Society*, 140(6), 1526–1533.

Garca, C.E., Prett, D.M., and Morari, M. (1989). Model predictive control: Theory and practice – a survey. *Automatica*, 25(3), 335 – 348.

Garcia, C.E. and Morshedi, A.M. (1986). Quadratic programming solution of dynamic matrix control (QDMC). *Chemical Engineering Communications*, 46(1-3), 73–87.

Hindmarsh, A.C., Brown, P.N., Grant, K.E., Lee, S.L., Serban, R., Shumaker, D.E., and Woodward, C.S. (2005). SUNDIALS: Suite of nonlinear and differential/algebraic equation solvers. *ACM Trans. Math. Softw.*, 31(3), 363–396.

Kumaresan, K., Sikha, G., and White, R.E. (2008). Thermal model for a Li-ion cell. *Journal of the Electrochemical Society*, 155(2), A164–A171.

Maciejowski, J.M. (2002). *Predictive Control: With Constraints*. Pearson Education.

Mesbah, A., Lakerveld, R., and Braatz, R.D. (2015). Plant-wide model predictive control of a continuous pharmaceutical manufacturing process. In *Proceedings of the American Control Conference*, 4301–4307.

Northrop, P.W.C., Ramadesigan, V., De, S., and Subramanian, V.R. (2011). Coordinate transformation, orthogonal collocation, model reformulation and simulation of electrochemical-thermal behavior of lithium-ion battery stacks. *Journal of The Electrochemical Society*, 158(12), A1461–A1477.

Peterson, T., Hernández, E., Arkun, Y., and Schork, F. (1992). A nonlinear DMC algorithm and its application to a semibatch polymerization reactor. *Chemical Engineering Science*, 47(4), 737–753.

Ramadass, P., Haran, B., Gomadam, P.M., White, R., and Popov, B.N. (2004). Development of first principles capacity fade model forLi-ion cells. *Journal of the Electrochemical Society*, 151(2), A196–A203.

Ramadass, P., Haran, B., White, R., and Popov, B.N. (2003). Mathematical modeling of the capacity fade of Li-ion cells. *Journal of Power Sources*, 123(2), 230–240.

Ramadesigan, V., Northrop, P.W., De, S., Santhanagopalan, S., Braatz, R.D., and Subramanian, V.R. (2012). Modeling and simulation of lithium-ion batteries from a systems engineering perspective. *Journal of The Electrochemical Society*, 159(3), R31–R45.

Rashid, M. and Gupta, A. (2014). Mathematical model for combined effect of SEI formation and gas evolution in Li-ion batteries. *ECS Electrochemistry Letters*, 3(10), A95–A98.

Sankarasubramanian, S. and Krishnamurthy, B. (2012). A capacity fade model for lithium-ion batteries including diffusion and kinetics. *Electrochimica Acta*, 70, 248–254.

Schiesser, W.E. (1991). *The Numerical Method of Lines*. Academic Press.

Torchio, M., Wolff, N.A., Raimondo, D.M., Magni, L., Krewer, U., Gopaluni, R.B., Paulson, J.A., and Braatz, R.D. (2015). Real-time model predictive control for the optimal charging of a lithium-ion battery. In *Proceedings of thet American Control Conference*, 4536–4541.

Van den Bossche, P., Vergels, F., Van Mierlo, J., Matheys, J., and Van Autenboer, W. (2006). SUBAT: An assessment of sustainable battery technology. *Journal of Power Sources*, 162(2), 913–919.

Zhang, Q. and White, R.E. (2008). Capacity fade analysis of a lithium ion cell. *Journal of Power Sources*, 179(2), 793–798.